

Node differentiation dynamics along the route to synchronization in complex networks

Christophe Letellier,^{1, a)} Irene Sendiña-Nadal,^{2, 3} Ludovico Minati,^{4, 5} and I. Leyva^{2, 3}

¹⁾ Rouen Normandie University — CORIA, Campus Universitaire du Madrillet, F-76800 Saint-Etienne du Rouvray, France ^{b)}

²⁾ Complex Systems Group & GISC, Universidad Rey Juan Carlos, 28933 Móstoles, Madrid, Spain ^{c)}

³⁾ Center for Biomedical Technology, Universidad Politécnica de Madrid, 28223 Pozuelo de Alarcón, Madrid, Spain

⁴⁾ Center for Mind/Brain Sciences (CIMEC), University of Trento, 38123 Trento, Italy

⁵⁾ Institute of Innovative Research, Tokyo Institute of Technology, Yokohama, 226-8503, Japan ^{d)}

(Dated: 22 February 2021)

Synchronization has been the subject of intense research during decades mainly focused on determining the structural and dynamical conditions driving a set of interacting units to a coherent state globally stable. However, little attention has been paid to the description of the dynamical development of each individual networked unit in the process towards the synchronization of the whole ensemble. In this paper, we show how in a network of identical dynamical systems, nodes belonging to the same degree class differentiate in the same manner visiting a sequence of states of diverse complexity along the route to synchronization independently on the global network structure. In particular, we observe, just after interaction starts pulling orbits from the initially uncoupled attractor, a general reduction of the complexity of the dynamics of all units being more pronounced in those with higher connectivity. In the weak coupling regime, when synchronization starts to build up, there is an increase in the dynamical complexity whose maximum is achieved, in general, first in the hubs due to their earlier synchronization with the mean field. For very strong coupling, just before complete synchronization, we found a hierarchical dynamical differentiation with lower degree nodes being the ones exhibiting the largest complexity departure. We unveil how this differentiation route holds for several models of nonlinear dynamics including toroidal chaos and how it depends on the coupling function. This study provides new insights to understand better strategies for network identification and control or to devise effective methods for network inference.

Keywords: Complex networks — Dynamical complexity — Route to synchronization — Chaos

I. INTRODUCTION

The description of networks can be structural, based on the characterization and modelling of their topological properties,^{1–3} or dynamical, usually referring to the collective behavior emerging from the interaction between node dynamics and the network architecture. Synchronization is the most thoroughly investigated ensemble dynamics,^{2,4,5} including a rich variety of related behaviours such as chimera states,^{6–8} cluster synchronization or⁹ explosive synchronization.^{10,11}

The route to the synchronous state has been approached from different points of view. Microscopically, it has been analyzed the different ways local synchronization grows as the coupling increases depending on the connectivity structure.^{4,12–14} Globally, the synchronizability of a population of identical networked oscillators, that is, the stability of the coherent state, has been

tackled through the master stability function and foresees the emergence of patterns when the stability of the network uniform state is lost.^{15–17}

While these approaches help to understand how synchronization clusters grow and eventually merge into a macroscopic coherent state or predict its stability for a particular network structure and coupling function, few works pay attention to the description of the nodal dynamics along the route to synchronization. Recently, it has been shown that the degree of complexity of the node dynamics is strongly dependent on the connectivity; in particular, the local connectedness appears to confer considerable node differentiation hallmarks, albeit following mechanisms that are intricate and delineate a non-monotonic effect.^{18–20} These ensemble fingerprints in the node dynamics can be used to infer the network statistical description, or even the detailed connectivity in certain conditions.²¹ By node differentiation it is here meant as the dynamical departure of an isolated node due to the interaction with its neighborhood, being more pronounced in networks with nodes having degree heterogeneity. In particular, a relatively large range of coupling strengths over which nodes with a higher degree have a less complex dynamics has been reported,¹⁹ ex-

^{a)} <http://www.atomosyd.net/spip.php?article1>

^{b)} Electronic mail: christophe.letellier@coria.fr

^{c)} Electronic mail: irene.sendina@urjc.es

^{d)} Electronic mail: lminati@ieee.org

plaining the low complexity observed in hubs of functional brain networks.²² However, the reverse situation, the existence of an even lower range of coupling strengths where high degree nodes are more complex than lower degree ones, remains under study.²⁰ The purpose of the present work is to elucidate the route of the node differentiation dynamics in a complex network before reaching a synchronous state, and, in particular, how it depends on the dynamical system, the coupling function and on the topological properties of the network structure.

In order to characterize and quantify this route to node differentiation dynamics as the coupling strength increases, we used the complexity measure recently introduced by Letellier *et al.*²³ able to distinguish organized from disorganized chaotic behavior together with maps of the dynamical patterns associated to relevant degree classes. Section II is devoted to introducing terminology and providing a brief description of the dynamical complexity measure. We then investigated in Section III the dynamical differences among Rössler oscillators in a star network according to their degree, and how those differences dependent upon the coupling function, the nominal dynamics, and the size of the star. In Section IV, we extended the analysis to star networks of dynamical systems featuring higher nominal complexity, namely the symmetric Lorenz system, the high-dimensional Mackey-Glass equation, and the toroidal Saito system, to determine whether a general scenario can be outlined. In Section V, we considered Rössler systems in larger networks to explore the node differentiation induced by embedding the oscillators in a much more complex topological environment. Finally, Section VI offers general conclusions.

II. DYNAMICAL COMPLEXITY MEASURE

Let us start by considering the general description of a network comprising N diffusively-coupled m -dimensional identical dynamical systems, whose state vector \mathbf{x}_i evolves as

$$\dot{\mathbf{x}}_i = \mathbf{f}(\mathbf{x}_i) - d \sum_{j=1}^N \mathcal{L}_{ij} \mathbf{h}(\mathbf{x}_j) \quad (1)$$

where $\mathbf{f}: \mathbb{R}^m \rightarrow \mathbb{R}^m$ and $\mathbf{h}: \mathbb{R}^m \rightarrow \mathbb{R}^m$ are the nominal dynamics — here, nominal refers to the vector field of the i -th nodal dynamics when isolated — and the coupling function, respectively, and d is the coupling strength. \mathcal{L}_{ij} are the elements of the Laplacian matrix encoding the network's connectivity, with $\mathcal{L}_{ii} = k_i$ the node degree, $\mathcal{L}_{ij} = -1$ if nodes i and j are connected, and $\mathcal{L}_{ij} = 0$ otherwise.

To characterize the nodal dynamics in a more reliable way, we computed a Poincaré section to the trajectory $\mathbf{x}_i(t)$ in the state space to rule out the local linear component and focus on the nonlinear signatures governing the dynamics.²⁴ Thus, for each oscillator, in the following, we computed a two-dimensional Poincaré section of

the attractor when the dynamics has a toroidal structure, or a first-return map built with one of the coordinates of the Poincaré section in case it is non-toroidal. Then, each oscillator's map is used to obtain a complexity coefficient C_D introduced in Ref.²³ and defined as

$$C_D = S_p + \Delta, \quad (2)$$

being S_p a permutation entropy and Δ a structurality marker. We chose this complexity definition because of its ability to distinguish organized unpredictable behavior (dissipative chaos) from disorganized unpredictable phenomena (noise or conservative chaos). While the entropy quantifies the unpredictability of the dynamics, the structurality accounts for its undescribability, two very different aspects contributing to the complexity of a dynamics.

The permutation entropy S_p is defined as in Ref.²⁵:

$$S_p = -\frac{1}{\log(N_s!)} \sum_{\pi} p_{\pi} \log p_{\pi} \in [0, 1]. \quad (3)$$

It is based on the probability distribution p_{π} of the $N_s!$ possible ordinal patterns constructed from the order relations of N_s successive data-points in the Poincaré section. The structurality is computed by dividing the first-return map (or the two-dimensional projection of the Poincaré section) into a $N_q \times N_q$ boxes and

$$\Delta = \sum_{i,j=1}^{N_q} \frac{q_{ij}}{N_q^2} \in [0, 1], \quad (4)$$

where $q_{ij} = 1$ if the box (i, j) is visited at least once, and $q_{ij} = 0$ otherwise. The structurality Δ is typically low ($\Delta < 0.2$) for organized dynamics, and large ($\Delta > 0.80$) for disorganized dynamics. We thus have $C_D \approx 0$ for a limit cycle ($S_p \approx 0$ and $\Delta \approx 0$), $0.5 < C_D < 1.0$ for dissipative chaotic behavior (organized but unpredictable), and $C_D > 1.5$ for weakly dissipative chaos or stochastic processes (both are unpredictable and disorganized).

In all our computations we used $N_s = 6$ as the length of the ordinal patterns. The number N_d of data points in the Poincaré section to compute S_p and Δ was $N_d = 10,000$, largely above the requirement $N_d > 5N_s!$ recommended by Riedl *et al.*²⁶ The number of boxes was $N_q = 5 \log(N_d)$ chosen such that $N_d \gg N_q$, as prescribed in Ref.²³. The box width δ_p is determined by the largest range visited in our simulations for a given system as $\delta_p = (x_{\max} - x_{\min})/N_q$, where x_{\max} and x_{\min} are the maximal and minimal values recorded along one axis of the first-return map. To avoid excessively promoting noise contamination or small fluctuations around period-1 limit cycle, we introduced a “noise filter” to interpret the ordered patterns of the N_s data points to allow permutation only if $|x_i - x_j| > \delta_p$.

Let us consider the paradigmatic Rössler system²⁷ to exemplify the ability of Eq.(2) to discriminate between different dynamics. The vector flow in Eq. (1) is

$$\mathbf{f}(\mathbf{x}) = [-y - z, x + ay, b + z(x - c)] \quad (5)$$

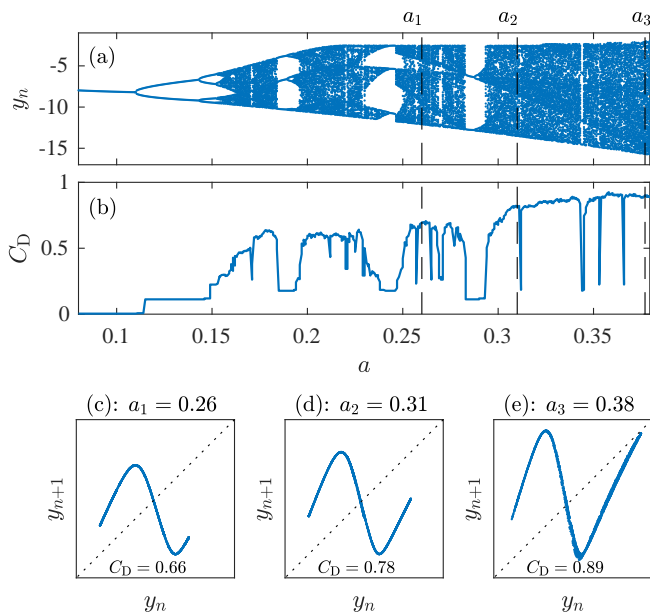


FIG. 1. Dynamical characterization of a single Rössler system upon variation of the a parameter and fixing $b = 0.2$ and $c = 5.7$. Bifurcation diagram using the Poincaré section \mathcal{P}_x (a) and dynamical complexity C_D (b). The dashed vertical lines in (a) and (b) are located at $a_1 = 0.26$, $a_2 = 0.31$, and $a_3 = 0.38$. The corresponding first-return maps from y_n are shown in (c)-(e) and their complexity values at the bottom of each panel.

taking $b = 0.2$ and $c = 5.7$ as fixed parameters and $a \in [0.08, 0.38]$ as the bifurcation parameter. Equation (1) was integrated using a fourth-order Runge-Kutta scheme²⁸ with a time step $\delta t = 0.01$. Initial conditions are randomly selected within a small neighborhood of radius 0.5 centered at the origin of the state space. Figure 1(a) shows the bifurcation diagram as a function of the parameter a for a single Rössler system ($d = 0$) computed from the y_n coordinate of the Poincaré section

$$\mathcal{P}_x \equiv \{(y_n, z_n) \in \mathbb{R}^2 \mid x_n = x_-, \dot{x}_n > 0\}, \quad (6)$$

where $x_- = (c - \sqrt{c^2 - 4ab})/2$ is the coordinate of the inner singular point.²⁹ The classical period-doubling cascade as a route to chaos is quantitatively characterized by the dynamical complexity C_D in Fig. 1(b). It perfectly captures the periodic windows ($C_D < 0.2$) intermingled with chaotic behavior. Panels (c)-(e) show the first-return maps for the three a values marked in (a)-(b) with vertical lines. The first value, $a = 0.26$ is located between a period-3 and a period-2 window and its first-return map is bimodal [Fig. 1(c)] but with a slightly developed third branch appearing just after the period-3 window. For $a = 0.31$, Fig. 1(d), the bimodal map has the three branches. A more developed chaos, characterized with three monotone branches, is observed for $a = 0.38$ in Fig. 1(e). In particular, the right end of the third branch approaches the vicinity of the bisecting line, indicating that a new period-1 orbit is about to be cre-

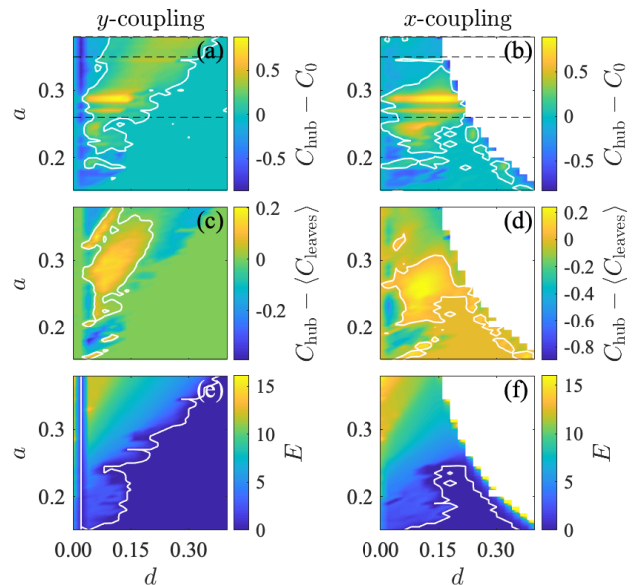


FIG. 2. Colormaps of the complexity values for a star of $N = 16$ coupled Rössler oscillators in the d - a parameter plane. Actual complexity change of the hub $C_{\text{hub}} - C_0$ (a)-(b) and the difference $C_{\text{hub}} - \langle C_{\text{leaves}} \rangle$ (c)-(d) when oscillators are coupled through the y (a,c), and x (b,d) variables, respectively. Bottom panels (e)-(f) show the synchronization error E . The color scales are provided on the right sides. In (a)-(f) panels, white curves are the corresponding null isolines, and horizontal dashed lines in (a)-(b) are plotted at $a = 0.26, 0.31$ and $a = 0.38$. White domains correspond to the ejection of the trajectory to infinity. Other parameter values are set as in Fig. 1.

ated in the population of unstable periodic orbits. This is the most developed chaos that can be observed along this line of the parameter space, as indicated by the dynamical complexity ($C_D = 0.89$), in agreement with the most developed first-return map.

III. A STAR NETWORK OF RÖSSLER SYSTEMS

Let us now consider a star network of N Rössler systems coupled according to Eq. (1), with $N - 1$ peripheral nodes and one central node acting as the hub, aiming at exploring the influence of the coupling function in the parameter space d - a . Top panels (a) and (b) of Fig. 2 show the actual change in complexity $C_{\text{hub}} - C_0$ of the hub in a $N = 16$ star with respect to the reference complexity value C_0 (which is a function of the parameter a) of an uncoupled node, for coupling schemes through variables y and x , respectively. Middle panels (c) and (d) provide the complexity difference between the hub and the leaves $C_{\text{hub}} - \langle C_{\text{leaves}} \rangle$.

From the colormaps, the first clear observation is that the coupling function has a role in the node differentiation dynamics, as reflected by the different distribution of complexity change on the a - d plane, which strongly depends on the network synchronizability. Panels (e,f)

in Fig.2 show the time-averaged synchronization error computed as

$$E = \frac{2}{N(N-1)} \sum_{i \neq j} \|\mathbf{x}_i - \mathbf{x}_j\|. \quad (7)$$

which is in agreement with the prediction given by the master stability function (MSF) for Rössler systems coupled through the y variable, type I synchronizability class -the MSF becomes negative above a critical value, and x variable, type II class -the MSF is negative in a bounded interval.^{15,30,31} For the particular network structure of a star of size $N = 16$, complete synchronization is indeed reached for a larger number of pairs (a,d) when Rössler systems are y -coupled than when x -coupled. In the latter case, full synchronization cannot be reached for $a \gtrsim 0.25$ before a boundary crisis ejects the trajectory to infinity (white domains in Fig. 2(f)). For this configuration, the location of $d\lambda_i$, being λ_i the i -th eigenvalue of the Laplacian matrix, is outside the range where the MSF is negative for any value of d , and the synchronous solution is always unstable.

Roughly, in the regions where the synchronization error is not null, for both x and y coupling, there is a large region of the parameter space with yellowish areas delimited by the white null isolines in panels in Figs. 2(a) and 2(b) where the effect of coupling is to render the dynamics of the hub more complex with respect to its uncoupled regime ($C_{\text{hub}} > C_0$). Outside this region, there are smaller islands (in blue) where the dynamics turns out to be less complex. However, when comparing this departure from the uncoupled dynamics between the hub and the leaves, Figs. 2(c) and 2(d), there are regions where the hub dynamics appears to be more complex than that of the leaves — for intermediate values of the coupling and of the parameter a — and regions where the opposite is realized. For example, for the y coupling, $C_{\text{hub}} < \langle C_{\text{leaves}} \rangle$ at the left and right side of the yellow region.

To analyse with further detail the dynamical differentiation of hub and leaves along the route to synchronization, we show in Fig. 3 cuts of the complexity difference $C_{j0} = C_j - C_0$, with $j = \{\text{hub}, \text{leaf}\}$ (black for the hub and red for one leaf) along the three horizontal dashed lines shown in Fig. 2(a). These curves clearly show that hub and leaf experience unlike differentiation routes before either the star synchronizes at d_c to the same dynamical state as in $d = 0$ for y -coupling [Fig. 3(a)-(d)] or it reaches a boundary crisis at d_b for the x coupling [Fig. 3(e)-(h)]. In all cases, the maximal differentiation occurs always before for the hub than for the leaf, that is, the maximum of the C_{j0} curves is located at a coupling that is lower for the hub than for the leaf. As it is shown at the inset of each panel, this shift coincides with the earlier synchronization of the hub to the mean field, here measured as

$$S_j = \langle \text{Re}(e^{i(\theta_j - \Phi)}) \rangle_t, \quad (8)$$

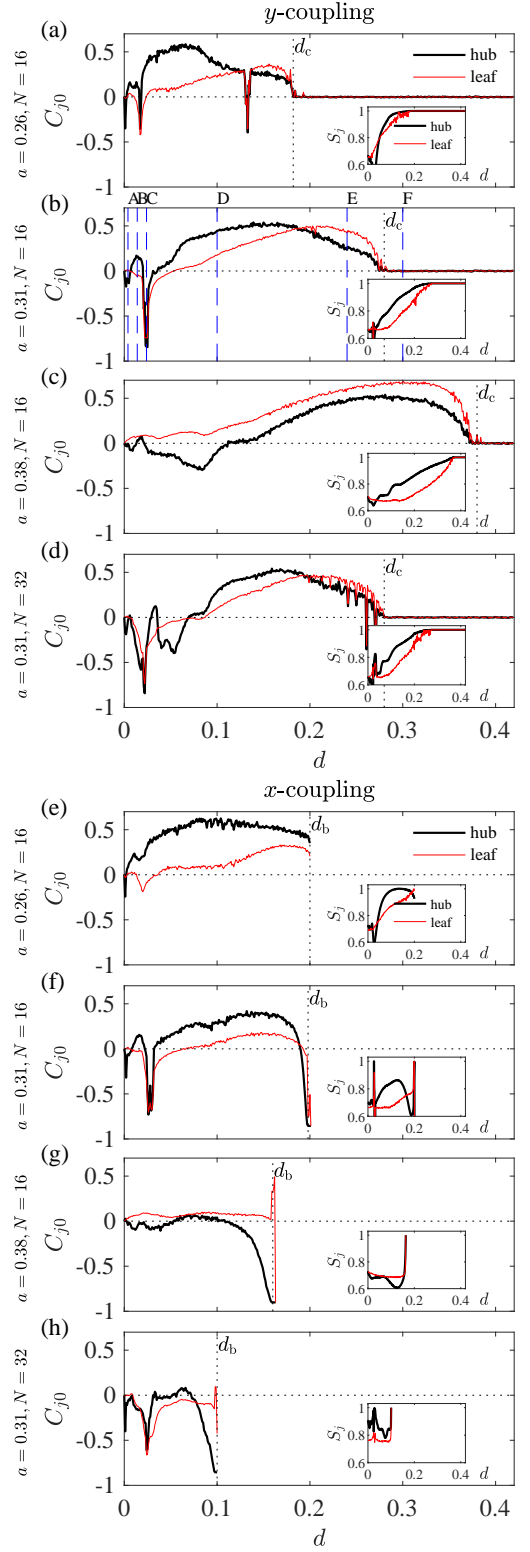


FIG. 3. Evolution of the relative complexity C_{j0} as a function of the coupling strength d for the hub (in black) and a leaf (in red) of a star network of y coupled (a)-(d) and x coupled (e)-(h) Rössler oscillators. (a,e) $a = 0.26$, (b,f) $a = 0.31$, and (c,g) $a = 0.38$ and $N = 16$. (d,h) $a = 0.31$ and $N = 32$. Insets in all panels show the phase synchronization S_j of the hub (black) and the leaf (red) with the mean field. Other parameter values: $b = 0.2$, and $c = 5.7$. One run per d -value.

being $\langle \dots \rangle_t$ the time average, Re stands for the real part, $\theta_j = \arctan(y_j/x_j)$ the phase of the $j = \text{hub/leaf}$, and Φ the mean-field global phase. By definition, $S_j \in [0, 1]$, and approaches 1 as the phase of the j -th oscillator is locked to the phase of the mean field.

Another observed systematic behavior is that, for increasing values of a , as the uncoupled dynamics is more developed (see Fig. 1), the relative complexity of the hub diminishes while increases for the leaf. Therefore, the relative position between the hub and leaf curves changes such that for $a = 0.26$ the hub's curve is almost always above the leaf's one, $C_{\text{hub},0} > C_{\text{leaf},0}$, while for $a = 0.38$, when the isolated dynamics is the most developed, the hub's curve is always below, $C_{\text{hub},0} < C_{\text{leaf},0}$. Another salient feature is that in the very weak coupling regime ($d < 0.05$), just after oscillators start interacting, there is a marked fall of the complexity with respect to C_0 for both hub and leaf. Finally, the impact of the size of the star is analysed in Fig. 3(d,h) for $N = 32$ and $a = 0.31$ which has to be compared with the panels (b) and (f) of the same figure for $N = 16$. Precisely, the hub complexity is slightly affected and only in the region of low coupling. As predicted by the MSF, for the y coupling, the threshold for synchronization d_c does only depend on the smallest non-zero eigenvalue λ_2 , which equals $\lambda_2 = 1$ in both configurations. On the other hand, for the x coupling, the boundary crisis is anticipated to smaller coupling values as the largest eigenvalue $\lambda_N = N$ increases with the size.

To picture the different dynamical states the hub and the leaf are visiting, we monitored their first-return maps at a specific points along the route to synchronization as shown in Fig. 3(b) with vertical dashed lines. Having in mind the map characterizing the uncoupled dynamics for $a = 0.31$ and shown in Fig. 1(d), for very low coupling [Fig. 4(A)], the leaf dynamics is nearly unaffected while the hub is exhibiting the presence of incoherent small perturbations and a shorter third branch. A slight increase in the coupling strength [Fig. 4(B)] amplifies this effect turning the hub's attractor into a very thick unimodal map and leaving the leaf's map almost unaltered. The next scenario [Fig. 4(C)] corresponds to the largest deviation from the uncoupled dynamics with both types of nodes displaying a much less complex dynamics. The hub is constrained to a small neighborhood of the inner singular point as revealed by the feeble cloud of points in the bisecting line. The leaf is locked on a period-2 limit cycle. Beyond this drop of complexity, the hub dynamics develops into a single huge cloud of points, displaced along the bisecting line towards the period-1 limit cycle [Fig. 4(D)]. The large complexity value attained by the hub $C_{\text{hub}} = 1.18 > 1$ indicates a very disorganized dynamics far from the typical noisy limit cycle. At the same time, the leaf moves into a first-return map with three thick branches due to the noisy feedback from the hub. Pursuing along the route to synchronization both hub and leaf each recover three branched maps slightly distorted until a synchronous state is recovered for $d > d_c$

in Fig. 4(F) and all nodes share the same dynamics as they had when uncoupled.

IV. STAR NETWORKS MADE OF OTHER DYNAMICAL SYSTEMS

A. Lorenz systems

Let us now consider the Lorenz 63 system³² whose vector flow in Eq. (1) is

$$\mathbf{f}(\mathbf{x}) = [\sigma(y - x), Rx - y - xz, -bz + xy] \quad (9)$$

which is equivariant under a rotation symmetry around the z -axis³³. This global property is the main difference with respect to the Rössler dynamics since, when the symmetry is modded out, the Lorenz attractor is topologically equivalent to the Rössler one.³³⁻³⁵ Lorenz systems coupled through variable y present a type-I synchronizability class and, therefore, complete synchronization is stable above a critical coupling threshold.

To compute the first-return map we proceeded as follows. The common Lorenz attractor for $R = 28$, resembling the two wings of a butterfly, is bounded by a genus-3 torus and the Poincaré section is the union of the two components

$$\mathcal{P}_{\pm} \equiv \{(y_n, z_n) \in \mathbb{R}^2 \mid x_n = \pm x_{\pm}, \dot{x}_n \lesseqgtr 0\} \quad (10)$$

where $x_{\pm} = \pm\sqrt{b(R-1)}$.^{34,36,37} The interval visited by each one of these components is normalized to the unit interval, and the component \mathcal{P}_- is shifted by -1 , leading to variable ρ . A quite close example of the first-return map for $R = 28$ is shown at the bottom of Fig. 5A featuring four branches paired due to the rotation symmetry.³⁸ The two increasing branches correspond to the reinjection of the trajectory into the wing from which it is issued, while the two decreasing branches are associated with the transition from one wing to the other. The two left (right) branches correspond to the n th intersection in the left (right) wing and to the $(n+1)$ th intersection in the left (right) or right (left) wing depending on the sign of the slope.

Figure 5 shows the relative complexity C_{j0} of the hub and a leaf of a $N = 32$ star network y -coupled Lorenz systems for two values of the parameter R . For $R = 28$, full synchronization is reached for $d_c \approx 2.22$. As with the Rössler systems, the complexity of the hub and leaves drop below C_0 in the weak coupling regime ($d \lesssim 1$) and beyond that point the hub becomes more complex than the nominal dynamics before full synchronization is eventually reached. For this parameter setting, the Lorenz hub experiences a sudden drop in complexity as illustrated in the first-return map [Fig. 5(A)]: while the hub dynamics is characterized by small fluctuations around the singular point in the centre of one of the wings, the leaves are nearly unperturbed with their four branches.

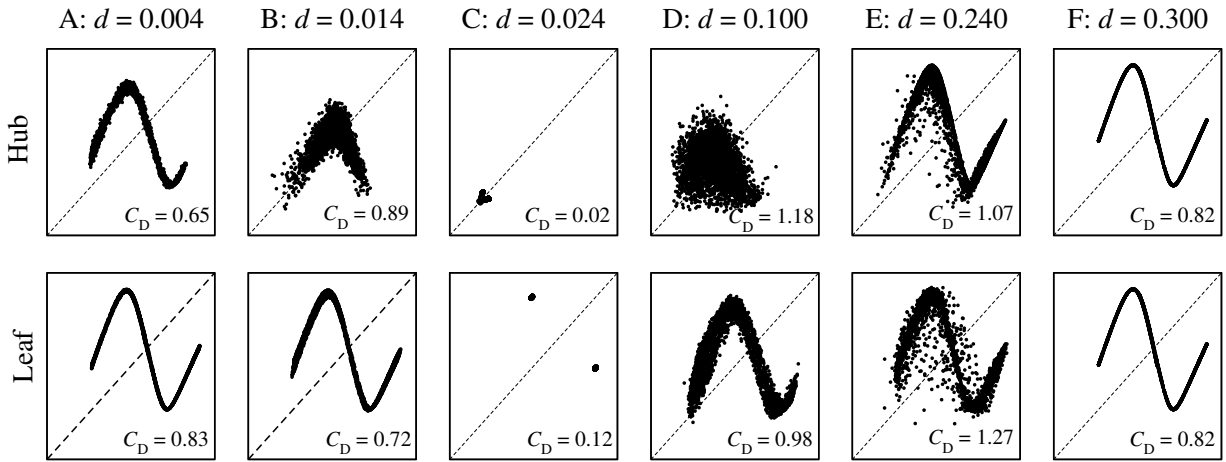


FIG. 4. First-return maps to the Poincaré section \mathcal{P} for the hub (top row) and one of the leaves (bottom row) in a star network of $N = 16$ y -coupled Rössler oscillators for $a = 0.31$ and for different d values. The corresponding complexities C_D are reported. The nominal complexity is $C_0 = 0.82$.

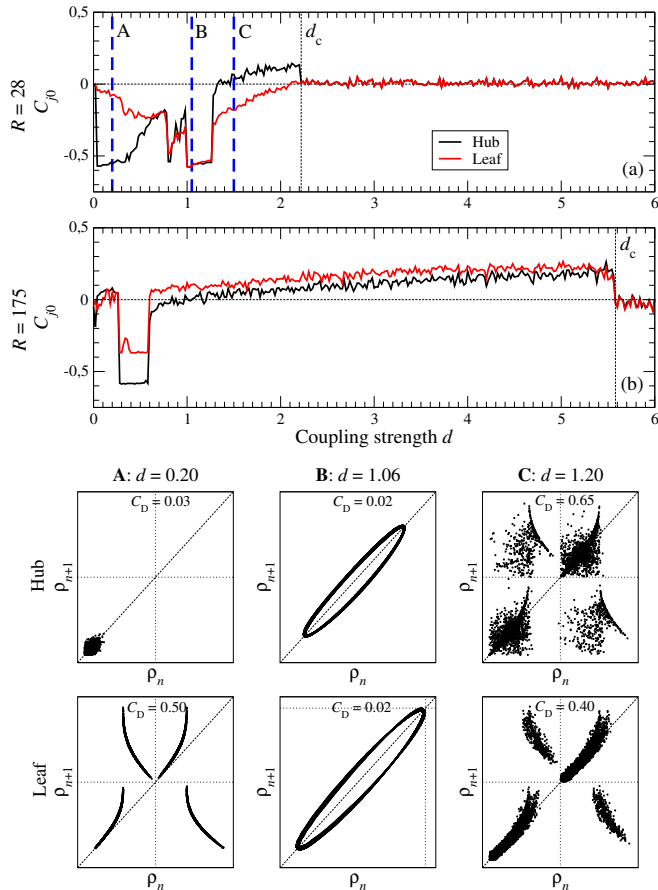


FIG. 5. (a)-(b) Relative complexity for the hub (black) and one of the leaves (red) as a function of the coupling strength d for a star network with $N = 32$ y -coupled Lorenz systems for two R -values. First-return maps of the hub (top) and of one leaf (bottom) for the cases A, B and C indicated by the blue dashed lines in the top panel. Other parameter values: $\sigma = 10$, $b = \frac{2}{3}$. A magnified view of the maps is plotted for the case B: the range used is not the same between the hub and leaf.

When d is further increased [Fig. 5(B)], the leaf dynamics also collapses, with all nodes surprisingly exhibiting a quasi-periodic dynamics, a regime not observed in an isolated Lorenz system. Notice that the size of the two tori are different. When the nodes' dynamics have topologically equivalent attractors (here, tori) but with a scaling factor, the phenomenon is known as *amplitude envelope synchronization*.³⁹ Finally, beyond this point of reduced dynamics and just before full synchronization [Fig. 5(C)], the interaction between hub and leaves moves the dynamics of the leaves again to the four paired branches although slightly more noisy than the uncoupled one, while the hub is strongly perturbed with a very disorganized dynamics. This scenario resembles the one observed for the Rössler system depicted in panel D of Fig. 4. Finally, we explored a second regime with an even more developed uncoupled dynamics for $R = 175$ whose first-return map has six branches (not shown). As in Fig. 3(c) for the Rössler system, the switch between the relative complexities of hub and leaf is no longer observed in Fig. 5 and the leaf curve is always above $C_{\text{leaf},0} > C_{\text{hub},0}$.

B. Mackey-Glass delay differential equation

It is possible to produce a chaotic attractor characterized by a smooth unimodal map via one-dimensional delay differential equations, for instance, the Mackey-Glass (MG) equation^{40,41}

$$\dot{x} = \mu \frac{x_\tau}{1 + x_\tau^p} - x_t \quad (11)$$

where x is the population of blood cells, $x_t = x(t)$ and $x_\tau = x(t - \tau)$. This equation was initially proposed for the control of hematopoiesis (the production of blood cells). Typically, the delay τ is the time-scale for proliferation and maturation of these blood cells. The di-

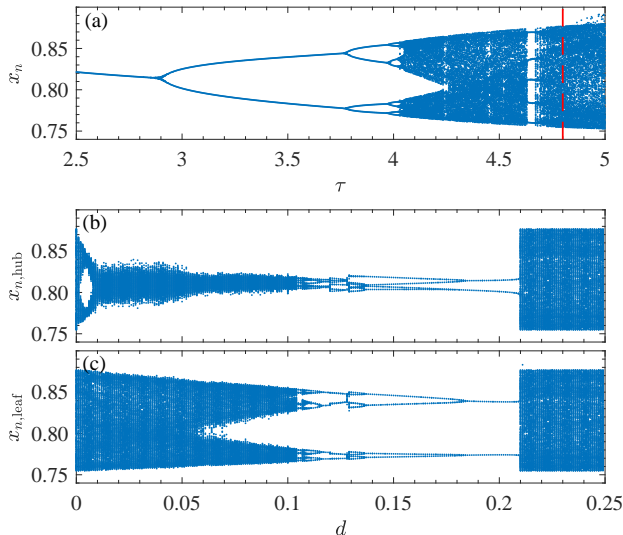


FIG. 6. (a) Bifurcation diagram for the Mackey-Glass delay differential equation (11) versus the time delay τ . (b-c) Bifurcation diagrams computed versus the coupling strength d for the hub and one of the leaves of a star network of $N = 32$ coupled Mackey-Glass equations (11) for $\tau = 4.8$ [see red-dashed vertical line in panel (a)]. For avoiding the multi-stability which is observed in such a network, the bifurcation diagram is computed without a reset of the initial condition at each new value of the coupling strength. Other parameter values are $\mu = 1.2$ and $p = 18.5$.

mension of the effective state space associated with a delay differential equation is dependent on the delay.^{42,43} Parameter values for parameters μ and p are such that a period-doubling cascade as a route to chaos is observed [Fig. 6(a)]. We chose a delay $\tau = 4.8$ (red dashed line in Fig. 6(a)) whose attractor is characterized by a smooth unimodal map with equivalent topological properties to the Rössler system. Increasing τ further leads to a much more complex behavior and computing a reliable Poincaré section is rather tricky.

Our goal here is to investigate the route to synchronization for unimodal dynamics produced by a potentially high-dimensional system. A network of MG systems can be fully synchronized using bidirectional coupling.⁴⁴

The attractor is bounded by a genus-1 torus and the single-component Poincaré section can be defined as

$$\mathcal{P}_{\text{MG}} \equiv \{x_n, \in \mathbb{R} \mid \dot{x}_n = 0.025, \ddot{x}_n > 0, x_n < 0.9\}. \quad (12)$$

The first-return map is one-dimensional and slightly foliated and quite similar to the one shown for the leaf in Fig. 7(A) for $N = 16$ coupled MG systems. Figure 7(a) shows the relative complexity of the hub and leaf as a function of the coupling strength. As observed in the Rössler and Lorenz systems, for low d -values, the hub experiences a sudden complexity drop while the leaves keep almost their nominal dynamics. As the coupling is increased, the hub starts synchronizing with the mean field and its relative complexity rises above 0. Beyond point B, all nodes reduce their complexity down to a

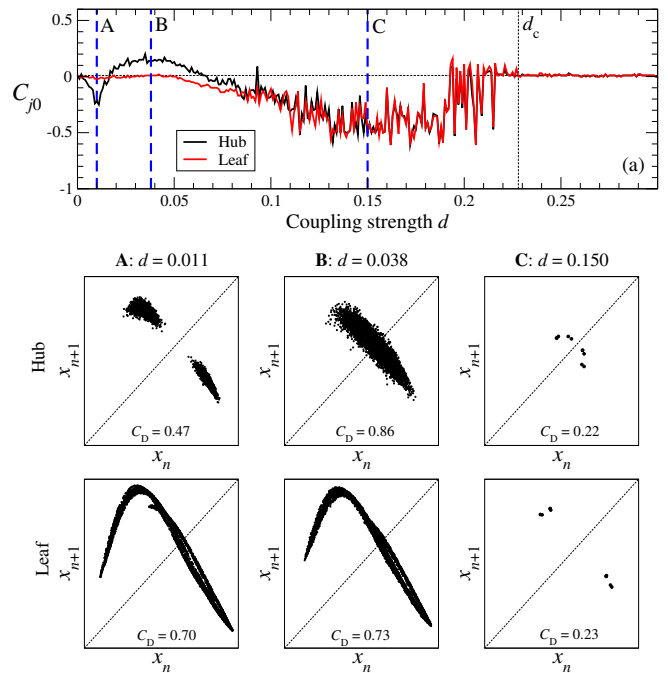


FIG. 7. (a) Relative complexity as a function of the coupling strength d for a star network of $N = 16$ coupled Mackey-Glass delay differential equations (11) for $\tau = 4.8$. (A)-(C) First-return maps of the hub (top) and of one leaf (bottom) for three different values of d . Other parameter values: $\mu = 1.2$ and $p = 18.5$.

minimal value (point C) before finally increasing up to full synchronization is reached. The noisy curves in that region is due to the extreme sensitivity to initial conditions found in this system. The maps for the hub and leaf [Figs. 7(A)-7(C)] corresponding to the setting points A, B, and C marked in Fig. 7(a) sketch the dynamical differentiation route.

The bifurcation diagrams for the hub and leaf respectively are computed as a function of the coupling d [Figs. 6(b)-6(c)]. In both cases, an inverse period-doubling cascade is observed up to a period-2 limit cycle is settled at $d = 0.18$. Curiously, the size of both limit cycles is different which, again, is an example of an amplitude envelope synchronization. The crisis leading to a larger chaotic attractor is strongly dependent on the initial conditions. In summary, the prevalent lines of the route to synchronization previously sketched are visible observed, albeit with some differences. Further investigations are necessary to fully understand their origin.

C. Four-dimensional Saito model

In this section, to confirm the generality of the nodal dynamical differentiation route, we will investigate a completely different model of nonlinear dynamics, the Saito model,⁴⁵ which is able to generate a very rich dynamical behavior including toroidal chaos. The vector

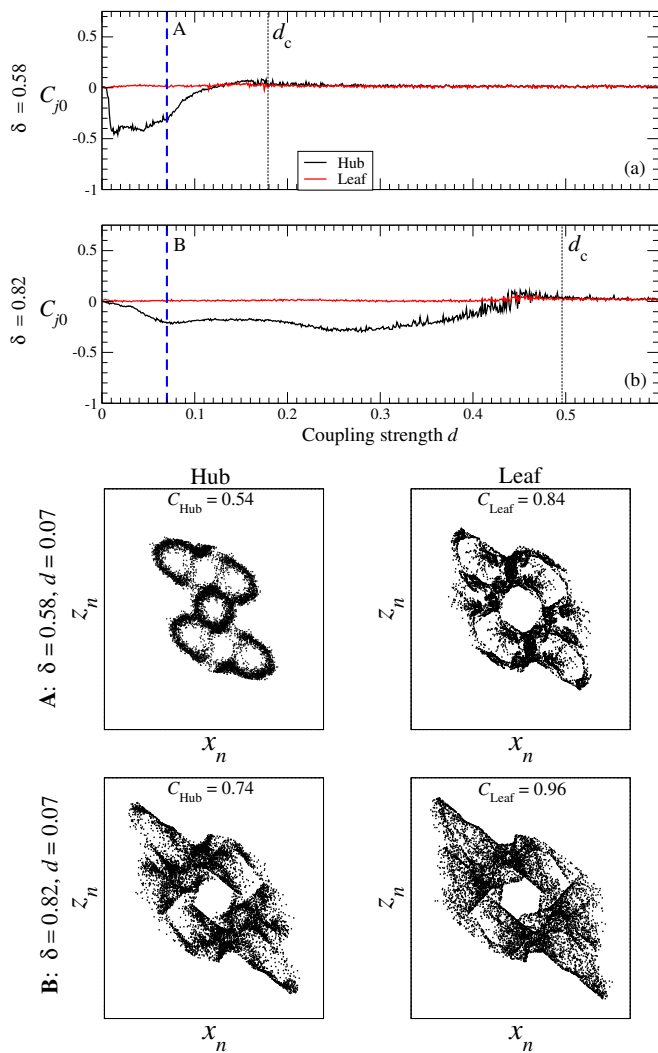


FIG. 8. Relative complexity C_{k0} as a function of the coupling strength d of a star network with $N = 16$ y -coupled Saito models (13) for (a) $\delta = 0.58$ and (b) $\delta = 0.82$. Poincaré sections for the hub and a leaf for (A) $\delta = 0.58$ and for (B) $\delta = 0.82$, both with $d = 0.07$. Other parameter values: $\rho = 14$, $\eta = 1$, and $\epsilon = 0.01$.

flow in Eq. (1) reads

$$\mathbf{f}(\mathbf{x}) = [\rho(-y + z), x + 2\delta y, -x - w, (z - \Phi(w))/\epsilon] \quad (13)$$

where $\mathbf{x} = (x, y, z, w)$ and

$$\Phi(w) = \begin{cases} w - (1 + \eta) & w \geq \eta \\ -\frac{w}{\eta} & \text{if } |w| < \eta \\ w + (1 + \eta) & w \leq -\eta. \end{cases} \quad (14)$$

This is a four-dimensional system involving a linear piecewise function as a switch mechanism. The dynamics produced by this model can be chaotic, quasi-periodic, toroidal chaotic, or even hyperchaotic, also structured around a torus. Parameters ρ , η , and ϵ are fixed and δ is used as a bifurcation parameter. Here we chose $\delta = 0.58$

for toroidal chaos, and $\delta = 82$ to produce hyperchaotic toroidal chaos. Close examples of the Poincaré sections of these attractors can be grasped, respectively, in Fig. 8(A) and 8(B) for a leaf of a star of $N = 16$ y -coupled Saito models whose dynamics are almost identical to the uncoupled scenarios. The main difference between these two dynamics is the “thickness” of the Poincaré section being much thinner for $\delta = 0.58$ than for $\delta = 0.82$. The hyperchaotic nature is revealed by the overlapping structures of the Poincaré section as observed in the folded-towel map introduced by Rössler.⁴⁶ This is partly confirmed with the Lyapunov exponents which for $\delta = 0.58$ are

$$\lambda_1 = 0.047 > \lambda_2 = 0.012 \approx \lambda_3 = -0.022 > \lambda_4 = -94.79,$$

with two null exponents as expected for toroidal chaos structured around a torus T^2 ,⁴⁷ and for $\delta = 0.82$ are

$$\lambda_1 = 0.164 > \lambda_2 = 0.069 \approx \lambda_3 = -0.033 > \lambda_4 = -94.70,$$

with two positive and one null exponents as needed for toroidal hyperchaos. Note that in the latter case it is still unclear whether the second positive exponent is merged or not with the third null exponent and this is an issue currently under study. Investigations, which are out of the scope of the present work, would allow determining whether the fourth dimension is required for embedding the toroidal chaos ($\delta = 0.58$). Being hyperchaotic for $\delta = 0.82$, the dynamics are necessarily four-dimensional.

When these models are coupled through the variable y , they synchronize as shown in Figs. 8(a) and 8(b) with the convergence of their relative complexity to zero, being the critical coupling d_c larger for the hyperchaotic dynamics. Nevertheless, in both cases, what is preserved along the route to synchronization with these toroidal chaotic and hyperchaotic dynamics is the node differentiation mainly of the hub whose dynamics turns less developed than the uncoupled one while the leaves sustain it over the whole range of coupling strengths [compare the first-return maps in Fig. 8(A), and in Fig. 8(B)]. The route to synchronization appears very simple, most likely due to the constrained toroidal structure of the nominal dynamics.

V. NETWORKS OF RÖSSLER OSCILLATORS

Having characterized the relationship between the degree centrality and dynamical complexity in star networks, we move forward to generalize our results to networks with a broader degree distribution. This issue was partially tackled in Refs.^{19,20}, where a strong correlation between degree k and complexity C_D allowed establishing a node hierarchy. However, given the present novel results revealing the important role played by the nominal nodal dynamics, we extend our present study to larger networks.

We maximize the degree heterogeneity by using Barabasi-Albert scale-free (SF) networks of N identical

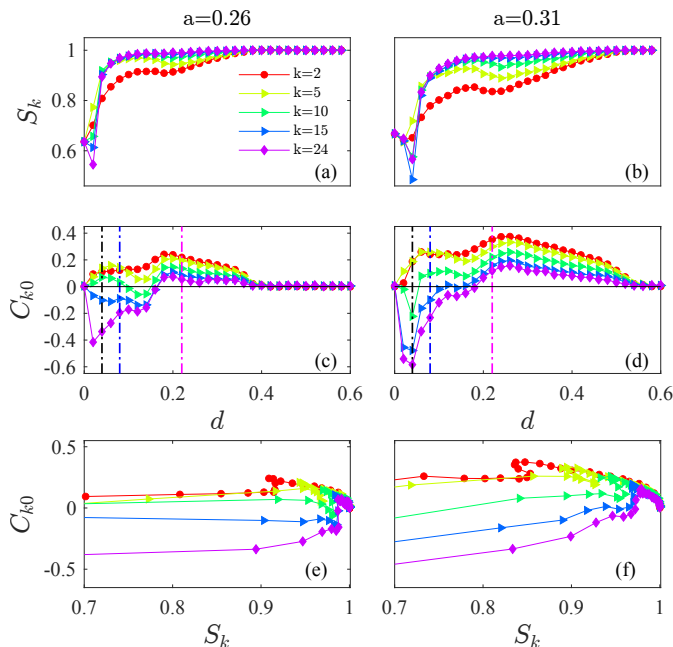


FIG. 9. (a,b) Average k -class S_k phase synchronization parameter for several values of degree k for $N = 300$, $\langle k \rangle = 4$ SF networks of y -coupled Rössler systems when $a = 0.26$ (left panels) and $a = 0.31$ (right panels), (c,d) averaged relative complexity C_{k0} . The vertical dotted lines mark the couplings analyzed in Fig. 10 the lower panels: $d = 0.04$ (black), $d = 0.08$ (blue) and $d = 0.22$ (magenta). (e,f) Relative complexity for different k -classes as a function of the phase synchronization S_k .

y -coupled Rössler oscillators retaining the parameter settings provided in Section III. Since we expect that nodes having the same degree k play equivalent roles in the network, we calculate the evolution of C_k within a degree class k by averaging over the N_k nodes having degree k , that is,

$$C_k = \frac{1}{N_k} \sum_{[j|k_j=k]} C_j, \quad (15)$$

where C_j is the dynamical complexity of the j th node. Here, we use the relative complexity $C_{k0} = C_k - C_0$ which helps to better assess the effects of both the coupling and the topology in the complexity of the k -class nodes. In addition, to evaluate the impact of the nodal environment, we perform our calculations for networks made of $N = 300$ nodes, wherein $\langle k \rangle = 4$. All the results are averaged over 10 different networks realizations.

First, in Fig. 9(a-b) we plot the time averaged phase synchronization S_k of k -class nodes with respect to the phase of the mean field for $N = 300$ SF networks as a function of the coupling d . We define S_k as

$$S_k = \frac{1}{N_k} \sum_{[j|k_j=k]} S_j. \quad (16)$$

where S_j is the time averaged phase synchronization of node j with the mean-field global phase, defined in

Eq. (8). The result is then ensemble averaged over 10 network realizations. Along the route to synchronization, the k -classes synchronize hierarchically to the mean field before all of them lock at the critical coupling ($d_c = 0.37$ for $a = 0.26$ and $d_c = 0.52$ for $a = 0.31$),^{19,48,49} therefore existing node differentiation also in heterogeneous networks. While the phase synchronization S_k is monotonously increasing for most of the coupling range and classes, the weakly coupled regime presents anomalous synchronization^{50,51} over which most of the S_k are below the basal, uncoupled level. This anomalous range, more prominent for $a = 0.31$, is associated with the maximal node differentiation [compare Fig. 9(b) and 9(d)].

As already observed in Section III, the less developed the dynamics, the smaller the critical value d_c [Fig. 9(c)-(d)]. In the weakly coupled regime, the relative complexity C_{k0} shows a strong node differentiation: while the hubs present a markedly reduced complexity with respect to the nominal value (with a clear negative minimal), for the smaller degrees the complexity increases. This increment in the less connected nodes ($k = 2$ and $k = 5$ in the example) is non-monotonous with d and k , as observed in the stars in Sections III and IV.

For stronger coupling all the nodes increase their complexity well above the nominal value, ordered following the reverse degree ranking [Fig. 9(c)-(d)], recovering the scenario observed for the hub in Section III. All these features are qualitatively shared for the two different a -values, but the deviations from the uncoupled value are larger for the more developed chaos, $a = 0.31$.

Plotting the relative complexity C_{k0} as a function of the phase synchronization S_k reveals a dependency which is stronger for nodes with a larger degree [Fig. 9(e)-(f)]. Typically, low-degree nodes exhibit a dynamics which is nearly independent of the synchronization while it is the opposite for large-degree nodes. It also clearly shows that the relative complexity converges to zero for larger d -values when k increases. This delineates another signature of node differentiation.

Therefore, we conclude that in most of the regimes it is possible to correlate the node degree with the relative complexity. Furthermore, the degree centrality is the single structural parameter that affects the node behaviour, while the rest of environmental topological features has no impact. This is shown in Fig. 10, where we plot the value of the relative complexity C_{k0} as a function of k for three representative values of d , both for SF networks and ER networks with $\langle k \rangle = 4$. The ER and SF curves overlap and, therefore, the dependence of C_k on a and d are the same regardless of the topology. This is quite remarkable since the ER and SF networks have a different critical coupling d_c : for a given d -value, their global dynamics are different, but the nodes of degree k have equivalent dynamics independently of the environment. The same result is obtained for different sizes of both ER and SF networks (not shown).

To better illustrate the node differentiation in larger networks, we plotted the first-return maps for three dif-

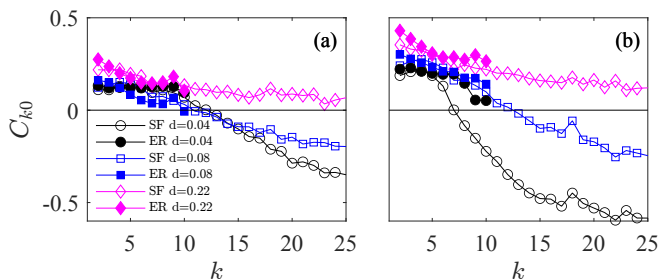


FIG. 10. Relative complexity C_{k0} as a function of the degree k for (a) $a = 0.26$, and (b) $a = 0.31$. In each panel, curves correspond to SF (void symbols) and ER (full symbols) with the coupling strengths marked in Fig.10(c,d) with vertical lines: $d = 0.04$ (circles), $d = 0.08$ (squares), and $d = 0.22$ (triangles). Results are averaged over 10 different network realizations of $N = 300$. Other parameter values as in Fig. 1.

ferent k -classes of nodes along the route to synchronization (Fig. 11). Low-degree nodes ($k = 2$) in SF networks produce first-return maps whose thickness increases with the coupling strength, up to $d < d_c$ (top row in Fig. 11): for these nodes, the relative complexity is always positive, and the first maps resemble the map of the uncoupled dynamics but thicker (compare with the map for $a = 0.31$ in Fig. 1). For large degree nodes (third row in Fig. 11), once the minimum complexity is reached in the weakly coupled regime, the complexity increases with the coupling strength d . Around the minimum, the maps comprise a small cloud of points in the neighborhood of the inner singular point (bottom left of the first-return map); this is progressively transformed into a “noisy” period-1 limit cycle, which is characterized by a cloud of points elongated perpendicularly to the bisecting line and located around the centre of the map ($d = 0.08$ with $C_{27} = 0.48$). Before the onset of synchronization, large degree nodes produce a map which resembles the nominal one but is slightly thicker ($d = 0.22$ with $C_{27} = 0.88$). The nodes with an intermediary degree ($k = 8$ in the example) produce a map which has features intermediate between the two extreme cases previously discussed: the node differentiation is, thus, evidently correlated with the node degree. As previously discussed, in large networks, node differentiation is mostly a monotonous function of the coupling strength and of the degree. When SF networks are replaced by ER ones, the degree range is narrower, but the maps for $k = 2$ and $k = 8$ are very similar to their counterparts in SF networks. We conclude that node degree is clearly the most important factor for the node differentiation along the route to synchronization.

VI. CONCLUSION

Routes to synchronization need to be elucidated to attain a better understanding and knowledge of the possible scenarios that may be encountered depending on the coupling, nominal node dynamics, topology, and network

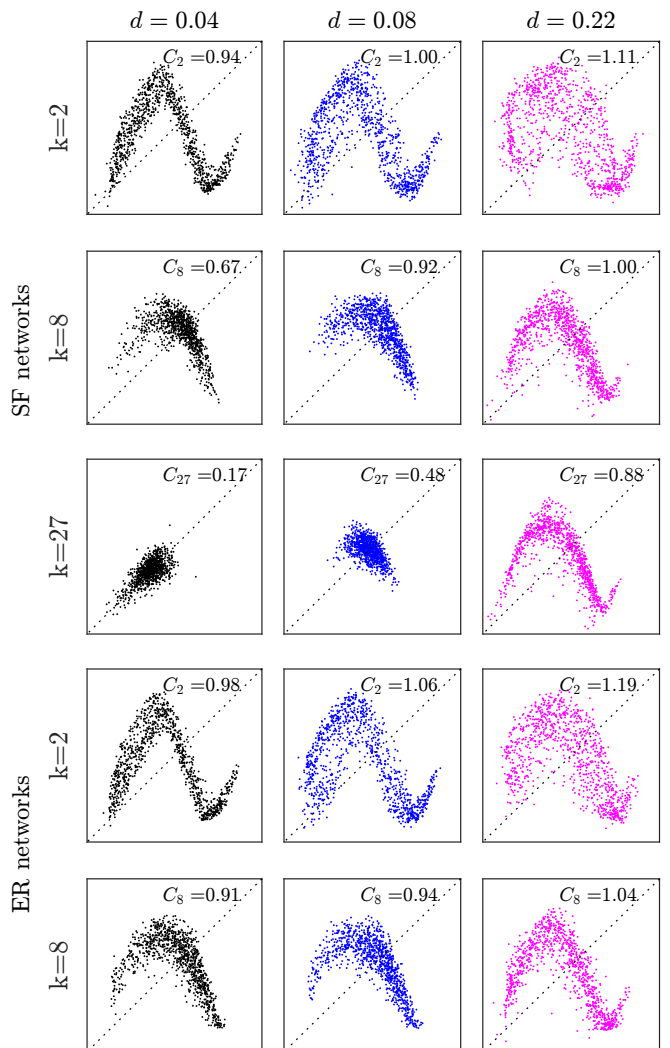


FIG. 11. Different first-return maps to a Poincaré section for three k -classes of nodes along a route to synchronization in a $N = 300$ ($\langle k \rangle = 4$) SF network of y -coupled Rössler nodes ($a = 0.31$ and other parameters as in Fig. 1). The complexity C_D is reported in each case.

size. Here, we confirmed and extended previous work depicting a non-trivial effect of connectedness on node dynamics, particularly the existence of a non-monotonic relationship between the complexity of node dynamics and coupling strength. There is, indeed, a node differentiation that evolves with the coupling strength. Typically, when the coupling function provides type-I synchronizability, low coupling strengths induce a significant reduction in the complexity of the large-degree nodes, while those having a small degree are left nearly unaffected. Consequently, increasing the d -value, all the nodes in small networks or those with a large degree in large networks present a minimal dynamical complexity. In every network, all nodes have a complexity that increases, often reaching a greater level than the nominal one, before the onset of full synchronization. This sketch for the route to synchronization is clearly observed for the two

three-dimensional systems (Rössler and Lorenz). With more complex node dynamics (Mackey-Glass and Saito), the decrease towards a minimal complexity is only observed in the hub of star networks; further studies with other network types are still needed for attaining a more general view of the latter system. The node differentiation is not a monotonic function of the coupling nor of the synchrony. When the coupling provides a type-II synchronizability, the route to synchronization is an abridged version of the route observed with a type-I synchronizability.

ACKNOWLEDGMENTS

ISN and IL acknowledge financial support from the Ministerio de Economía, Industria y Competitividad of Spain under project FIS2017-84151-P.

- ¹M. E. J. Newman, “The structure and function of complex networks,” *SIAM Review* **45**, 167–256 (2003).
- ²S. Boccaletti, V. Latora, Y. Moreno, M. Chavez, and D.-U. Hwang, “Complex networks: Structure and dynamics,” *Physics Reports* **424**, 175–308 (2006).
- ³S. Boccaletti, G. Bianconi, R. Criado, C. del Genio, J. Gómez-Gardeñes, M. Romance, I. Sendiña-Nadal, Z. Wang, and M. Zanin, “The structure and dynamics of multilayer networks,” *Physics Reports* **544**, 1–122 (2014).
- ⁴A. Arenas, A. Díaz-Guilera, and C. J. Pérez-Vicente, “Synchronization processes in complex networks,” *Physica D* **224**, 27–34 (2006).
- ⁵F. A. Rodrigues, T. K. D. Peron, P. Ji, and J. Kurths, “The Kuramoto model in complex networks,” *Physics Reports* **610**, 1–98 (2016).
- ⁶Y. Kuramoto and D. Battogtokh, “Coexistence of coherence and incoherence in nonlocally coupled phase oscillators,” *Nonlinear Phenomena in Complex Systems* **5**, 380–385 (2002).
- ⁷D. M. Abrams and S. H. Strogatz, “Chimera states for coupled oscillators,” *Physical Review Letters* **93**, 174102 (2004).
- ⁸A. M. Hagerstrom, T. E. Murphy, R. Roy, P. Hövel, I. Omelchenko, and E. Schöll, “Experimental observation of chimeras in coupled-map lattices,” *Nature Physics* **8**, 658–661 (2012).
- ⁹L. M. Pecora, F. Sorrentino, A. M. Hagerstrom, T. E. Murphy, and R. Roy, “Cluster synchronization and isolated desynchronization in complex networks with symmetries,” *Nature Communications* **5**, 4079 (2014).
- ¹⁰J. Gómez-Gardenes, S. Gómez, A. Arenas, and Y. Moreno, “Explosive synchronization transitions in scale-free networks,” *Physical Review Letters* **106**, 128701 (2011).
- ¹¹I. Leyva, I. Sendiña-Nadal, J. Almendral, A. Navas, S. Olmi, and S. Boccaletti, “Explosive synchronization in weighted complex networks,” *Physical Review E* **88**, 042808 (2013).
- ¹²J. G. Restrepo, E. Ott, and B. R. Hunt, “Synchronization in large directed networks of coupled phase oscillators,” *Chaos* **16**, 015107 (2006).
- ¹³J. Gómez-Gardeñes, Y. Moreno, and A. Arenas, “Paths to synchronization on complex networks,” *Physical Review Letters* **98**, 034101 (2007).
- ¹⁴T. Pereira, S. van Strien, and M. Tanzi, “Heterogeneously coupled maps: hub dynamics and emergence across connectivity layers,” *Journal of the European Mathematical Society* **22**, 2183–2252 (2020).
- ¹⁵L. M. Pecora and T. L. Carroll, “Master stability functions for synchronized coupled systems,” *Physical Review Letters* **80**, 2109–2112 (1998).
- ¹⁶M. Barahona and L. M. Pecora, “Synchronization in small-world systems,” *Physical Review Letters* **89**, 054101 (2002).
- ¹⁷L. M. Pecora, “Synchronization of oscillators in complex networks,” *Pramana* **70**, 1175–1198 (2008).
- ¹⁸A. Tlaie, I. Leyva, R. Sevilla-Escoboza, V. P. Vera-Avila, and I. Sendiña-Nadal, “Dynamical complexity as a proxy for the network degree distribution,” *Physical Review E* **99**, 012310 (2019).
- ¹⁹A. Tlaie, L. M. Ballesteros-Esteban, I. Leyva, and I. Sendiña-Nadal, “Statistical complexity and connectivity relationship in cultured neural networks,” *Chaos, Solitons & Fractals* **119**, 284–290 (2019).
- ²⁰L. Minati, H. Ito, A. Perinelli, L. Ricci, L. Faes, N. Yoshimura, Y. Koike, and M. Frasca, “Connectivity influences on nonlinear dynamics in weakly-synchronized networks: Insights from Rössler systems, electronic chaotic oscillators, model and biological neurons,” *IEEE Access* **7**, 174793–174821 (2019).
- ²¹D. Eroglu, M. Tanzi, S. van Strien, and T. Pereira, “Revealing dynamics, communities, and criticality from data,” *Physical Review X* **10**, 021047 (2020).
- ²²J. H. Martínez, M. E. López, P. Ariza, M. Chavez, J. A. Pineda-Pardo, D. López-Sanz, P. Gil, F. Maestú, and J. M. Buldú, “Functional brain networks reveal the existence of cognitive reserve and the interplay between network topology and dynamics,” *Scientific reports* **8**, 10525 (2018).
- ²³C. Letellier, I. Leyva, and I. Sendiña-Nadal, “Dynamical complexity measure to distinguish organized from disorganized dynamics,” *Physical Review E* **101**, 022204 (2020).
- ²⁴C. Letellier, “Estimating the Shannon entropy: Recurrence plots versus symbolic dynamics,” *Physical Review Letters* **96**, 254102 (2006).
- ²⁵C. Bandt and B. Pompe, “Permutation entropy: A natural complexity measure for time series,” *Physical Review Letters* **88**, 174102 (2002).
- ²⁶M. Riedl, A. Müller, and N. Wessel, “Practical considerations of permutation entropy,” *European Physical Journal Special Topics* **222**, 249–262 (2013).
- ²⁷O. E. Rössler, “An equation for continuous chaos,” *Physics Letters A* **57**, 397–398 (1976).
- ²⁸W. H. Press, S. A. Teukolsky, and W. T. V. B. P. Flannery, *Numerical Recipes in C. The Art of Scientific Computing*, 2nd ed. (Cambridge University Press, Cambridge, New York, Port Chester, Melbourne, Sydney, 1992).
- ²⁹C. Letellier, P. Dutertre, and B. Maheu, “Unstable periodic orbits and templates of the Rössler system: Toward a systematic topological characterization,” *Chaos* **5**, 271–282 (1995).
- ³⁰L. Huang, Q. Chen, Y.-C. Lai, and L. M. Pecora, “Generic behavior of master-stability functions in coupled nonlinear dynamical systems,” *Physical Review E* **80**, 036204 (2009).
- ³¹I. Sendiña-Nadal, S. Boccaletti, and C. Letellier, “Observability coefficients for predicting the class of synchronizability from the algebraic structure of the local oscillators,” *Physical Review E* **94**, 042205 (2016).
- ³²E. N. Lorenz, “Deterministic nonperiodic flow,” *Journal of the Atmospheric Sciences* **20**, 130–141 (1963).
- ³³C. Letellier and R. Gilmore, “Covering dynamical systems: Two-fold covers,” *Physical Review E* **63**, 016206 (2001).
- ³⁴C. Letellier, P. Dutertre, and G. Gouesbet, “Characterization of the Lorenz system, taking into account the equivariance of the vector field,” *Physical Review E* **49**, 3492–3495 (1994).
- ³⁵C. Letellier, *Caractérisation topologique et reconstruction des attracteurs étranges*, Ph.D. thesis, University of Paris VII, Paris, France (1994).
- ³⁶T. D. Sankov and R. Gilmore, “Topological aspects of the structure of chaotic attractors in \mathbb{R}^3 ,” *Physical Review E* **69**, 056206 (2004).
- ³⁷C. Letellier, L. A. Aguirre, and J. Maquet, “Relation between observability and differential embeddings for nonlinear dynamics,” *Physical Review E* **71**, 066213 (2005).
- ³⁸G. Byrne, R. Gilmore, and C. Letellier, “Distinguishing between folding and tearing mechanisms in strange attractors,” *Physical*

- Review E **70**, 056214 (2004).
- ³⁹J. M. Gonzalez-Miranda, “Amplitude envelope synchronization in coupled chaotic oscillators,” *Physical Review E* **65**, 036232 (2002).
- ⁴⁰M. C. Mackey and L. Glass, “Oscillation and chaos in physiological control systems,” *Science* **197**, 287–289 (1977).
- ⁴¹L. Glass and M. C. Mackey, “Pathological conditions resulting from instabilities in physiological control system,” *Annals of the New York Academy of Sciences* **316**, 214–235 (1979).
- ⁴²I. Gumowski, “Sensitivity of certain dynamic systems with respect to a small delay,” *Automatica* **10**, 659–674 (1974).
- ⁴³J. D. Farmer, “Chaotic attractors of an infinite-dimensional dynamical system,” *Physica D* **4**, 366–393 (1982).
- ⁴⁴K. Pyragas, “Synchronization of coupled time-delay systems: Analytical estimations,” *Physical Review E* **58**, 3067–3071 (1998).
- ⁴⁵T. Saito, “An approach toward higher dimensional hysteresis chaos generators,” *IEEE Transactions on Circuits and Systems* **37**, 399–409 (1990).
- ⁴⁶O. E. Rössler, “Chaos,” in *Structural Stability in Physics*, edited by G. Güttinger and H. Eikemeier (Springer, Berlin Heidelberg, 1979) pp. 290–309, proceedings of Two International Symposia on Applications of Catastrophe Theory and Topological Concepts in Physics Tübingen, May 2-6 and December 11-14, 1978.
- ⁴⁷C. Letellier and O. E. Rössler, “Chaos: The world of nonperiodic oscillations,” (Springer, Cham, Switzerland, 2020) Chap. An updated hierarchy of chaos, pp. 181–203.
- ⁴⁸C. Zhou and J. Kurths, “Hierarchical synchronization in complex networks with heterogeneous degrees,” *Chaos* **16**, 015104 (2006).
- ⁴⁹T. Pereira, “Hub synchronization in scale-free networks,” *Physical Review E* **82**, 036201 (2010).
- ⁵⁰B. Blasius, E. Montbrió, and J. Kurths, “Anomalous phase synchronization in populations of nonidentical oscillators,” *Physical Review E* **67**, 035204 (2003).
- ⁵¹B. Boaretto, R. Budzinski, T. Prado, J. Kurths, and S. Lopes, “Neuron dynamics variability and anomalous phase synchronization of neural networks,” *Chaos* **28**, 106304 (2018).